PHYSICAL REVIEW B VOLUME 12, NUMBER 10 15 NOVEMBER 1975

Surface-plasmon dispersion on the (100) face of aluminum

C. B. Duke and L. Pietronero*
Webster Research Center, Xerox Corporation, 800 Phillips Road, Webster, New York 14580

J. O. Porteus
Physics Division, Michelson Laboratory, China Lake, California 93555

J. F. Wendelken†
Coordinated Science Laboratory, University of Illinois, Urbana, Illinois 61801
(Received 10 March 1975)

Measurements of the inelastic low-energy ($20 \lesssim E \lesssim 200$ eV) electron-diffraction intensities from Al(100) are reported and analyzed to extract the dispersion relation of surface plasmons on this face of aluminum. Examination of five independent sets of experimental intensities using the two-step model of inelastic diffraction leads to the preferred results $\hbar\omega_s(p_\parallel) = 10.4(\pm 0.1) - 2(\pm 1)p_\parallel + 9(\pm 3)p_\parallel^2$, and $\Gamma_s(p_\parallel) = 1.2(\pm 0.5) + 1(\pm 0.5)p_\parallel$ for the surface-plasmon dispersion and damping, respectively. Momenta are measured in Å^{-1} and energies in eV. The analytical procedure utilized to extract surface-plasmon dispersion relations is modified, and our prior analyses for Al(111) are corrected by incorporating these modifications. Comparison of the surface-plasmon dispersion on Al(100) with that on Al(111) reveals that Al(100) is associated with a flatter dispersion and smaller damping. Within experimental error $\hbar\omega_s(p_\parallel = 0)$ is the same for both faces. Comparison of the measured dispersion relations with calculated ones reveals the clear failure of all models based on either step-function electron densities or electrons confined by an infinite surface potential barrier. Both bulk-scattering processes and the detailed shape of the electron density profile at the surface must be incorporated into any microscopic model which is proposed for the quantitative description of the surface-plasmon dispersion relations obtained from our analyses.

I. INTRODUCTION

Although aluminum is a nearly-free-electron metal, elementary arguments[1-3] suggest that the electronic-charge-density profiles on its various faces should differ. Since the dispersion relation of surface plasmons is thought to be a direct measure of such differences,[4-11] we have undertaken to measure these dispersion relations on the two closest-packed faces, i.e., (111) and (100), of aluminum. We utilize the method of measuring[12-19] inelastic low-energy electron diffraction (ILEED) intensities for electrons diffracted with energy losses $20 \lesssim w \lesssim 17$ eV from these faces, and analyzing these intensities using the two-step inelastic-collision model.[20-23] The results for epitaxially grown films of aluminum with the (111) orientation have been presented earlier.[24,25] Since the elastic low-energy electron diffraction (ELEED) data from single-crystal Al(111) differ negligibly from those for the Al(111) films,[19] however, we do not pursue Al(111) analysis further. In this paper we examine comparable data taken for Al(100),[17,19] and analyze them to determine the surface-plasmon dispersion relation for this face. A preliminary report of this work has been given elsewhere.[26]

We proceed by reviewing briefly in Sec. II the nature of our sample preparation and data collection procedures, and indicating the extent of the data base for Al(100). The analysis of these data is described in Sec. III. The resulting surface-plasmon dispersion relations are summarized in Sec. IV. The paper concludes with a discussion of both the analysis procedure *per se*, and the consequences of the differences which we discern between surface-plasmon dispersion on Al(100) and Al(111).

II. EXPERIMENTAL PROCEDURE

Since a major objective of our work is the establishment of the accuracy with which surface-plasmon dispersion relations may be extracted from experimental inelastic-low-energy-electron-diffraction (ILEED) intensity data, we decided to base this analysis on independent sets of data taken at two different laboratories. Thus, in this section we initially review the experimental procedure used at the China-Lake (Porteus) and University of Illinois (Wendelken) Laboratories, respectively, and conclude by specifying the extent of the data base acquired. Detailed presentations of these data are given elsewhere.[17,19]

Both the sample preparation[18] and data collection[16] procedures used in this work at the China Lake laboratories already have been published. Briefly, aluminum single crystals were reduced to the form of $\frac{3}{8}$-in.-diam disk using a spark cutter. A recessed mounting shoulder was provided around the disk perimeter to avoid contamination during sputter cleaning. The surface was ground and polished to within 0.01° of the desired crystal planes as determined using an x-ray goniometer.

Each crystal was electropolished in perchloric acid-ethanol solution immediately before mounting in the vacuum chamber. Residual oxide and other contaminants were then removed by equal time intervals of argon-ion sputtering and annealing at 500 °C. Only 4–6 h of sputtering were required to reduce contaminant Auger peaks below detectable limits. After the initial cleaning less than 1 h each of sputtering and annealing was required to reclean the surface. The sample was allowed to cool to 100 °C before any observations were made. The diffractometer utilized to perform the ILEED intensity measurements is that described by Porteus and Faith,[16] modified by the inclusion of a new sample preparation chamber.[19] The computer differentiation scheme outlined in Ref. 16 was employed to obtain experimental loss profiles (the derivative of the secondary emission into a fixed direction as a function of the loss energy $w = E - E'$, as defined by Laramore and Duke[27,28]). The energy-loss resolution achieved by the retarding voltage stepper is $400 \lesssim w \lesssim 100$ meV for the data utilized herein. The absolute accuracy of the loss profile is ± 100 meV; the $w \equiv 0$ loss profile being normalized to an independently measured energy profile of an elastically scattered beam.[16]

In the case of the data taken at Illinois, the target was a macroscopic Al(100) single crystal with the dimensions $1\frac{3}{8} \times \frac{3}{8} \times \frac{1}{8}$ in^3. Preparation of the target began with grinding of the (100) face with 15 μm levigated alumina to an accuracy of better than 0.10 deg as determined through the use of an x-ray diffractometer and a special grinding jig.[17] Tilt planes with a tilt separation on the order of 0.10 deg were found to be a common occurrence in the aluminum targets tested, however, so a region 0.2 in. in diameter free of tilt planes was chosen as the target surface. After etching with HF, final grinding of the surface was completed using 1-μm levigated alumina. The target was then chemically polished in a solution of phosphoric, sulfuric, and nitric acids and electropolished in a perchloric acid solution.[17] After installation in a vacuum chamber, which provides a vacuum of better than 1×10^{-10} Torr, the target was cleaned *in situ* by bombarding the surface with 500-eV neon ions at an angle of incidence of 55 deg from the target normal. The data were taken after at least 20 h of ion bombardment administered in small doses followed by annealing. During the course of the data taking the target was given a daily 30-min ion bombardment followed by a 1-h annealing period. The surface then remained suitably clean for at least 8 h when the target was at 300 °K and for 2 h when the target was at 100 °K. "Suitably clean" means that no changes occurred in the LEED results and no contamination was evident when the Auger spectra were observed.

The Illinois data were obtained using a custom-built high-resolution ($30 \leq \Delta E \leq 300$ meV, $\Delta\theta = 1$ deg) low-energy electron diffractometer which is described elsewhere.[17] For the measurements involving the surface plasmons, an energy resolution of 100 meV was utilized. Following the target cleaning procedures just described, the instrument calibration was checked and the target contact potential was compensated for at the temperature used during the measurements. Elastic intensity profiles,[27,28] were obtained at various temperatures. Then, using primary beam energies of E_0 and $E_0 + 7$ eV (where E_0 is the energy of a resonance in the elastic intensities) loss profiles were obtained in the specular beam direction, and also with the collector located in 1-deg increments up to 6 deg above and below the specular direction and in 2-deg increments up to 15 deg above and below the specular direction. Inelastic angular profiles[27,28] were obtained in 1-V increments in the loss energy for $w = 8$–16 eV. This procedure was repeated for each resonance studied. Both loss profiles and angular profiles were obtained directly from the instrument in continuous, motor-driven sweeps. The output was obtained in a pulse counting mode using an electron multiplier and ratemeter connected to an X-Y recorder.

As emphasized earlier[23,25,28] and reviewed in Sec. III, a substantial body of elastic-low-energy-electron-diffraction (ELEED) intensity data must be taken in order to select the region of incident beam parameters[28] (energy, E; polar angle, θ; and azimuthal angle, ϕ) in which to examine the ILEED intensity. A synopsis of the data obtained for this purpose (and available from the authors upon request) is presented in Table I. Similarly, in Table II we summarize all of the ILEED intensity measurements performed for this study,[17,19] and in Table III the subsets of these data utilized in our analysis of surface-plasmon dispersion.

III. DATA ANALYSIS

Our discussion of the procedure utilized to analyze the data summarized in Tables I–III is divided into three parts. First, we review the nature of the model Hamiltonian[22,23,27] and of the analytical procedure.[23,25] Second, we describe the selection of those incident beam parameters, (E, θ, ϕ), for which the inelastic-low-energy-electron-diffraction (ILEED) intensities were measured and analyzed. Finally, we specify the background-subtraction and plasmon damping parameters utilized during our analysis of the real part of the surface-plasmon dispersion relation.

The analytical procedure which we employ was proposed by Duke and Landman and, consequently, is described in detail in their papers.[23,25] An incident free electron is taken to scatter once

TABLE I. Elastic-low-energy–electron-diffraction intensities for Al(100) used to select ranges of incident beam parameters for use in the determination of surface-plasmon dispersion relations from inelastic low-energy electron diffraction. Azimuth is measured relative to the side of a primitive surface unit cell.

ϕ (Azimuth)	$\theta_0(\Delta\theta)\theta_1$ (Range of polar angles)	E_0-E_1 (Energy range, eV)	T (Temperature, °K)	Reference for raw data
0	13°(2°)27°	30–200	300	19
0	5°(5°)25°	20–250	85	17
0	19°(2°)27°	20–250	100	17
15°	5°(5°)15°	20–250	400	17
15°	5°(5°)15°	20–250	300	17
15°	5°(5°)25°	20–250	85	17
15°	11°(2°)19°	20–250	100	17
18.4°	9°(2°)29°	30–200	300	19
26.6°	9°(2°)29°	30–200	300	19
45°	9°(2°)29°	30–200	300	19
45°	5°(5°)25°	20–250	85	17

elastically from the ion cores of the target and once inelastically by virtue of either bulk or surface-plasmon creation. The expression for the elastic scattering vertex is given by Eq. (4) in Ref. 23 with the phase shifts calculated using an overlapping atomic charge-density model[29] and

TABLE II. Reference list of all ILEED intensity data for the (00) beam of electrons diffracted from Al(100) obtained for possible analysis of surface-plasmon dispersion.

Incident beam parameters E (eV)	ϕ	θ	Temperature T (°K)	Loss-energy range $w_0(\Delta w)w_1$ (eV)	Exit angle range $\theta_0'(\Delta\theta')\theta_1'$	Data reference
132	0	15	300	7(0.4)18	0(2)30	19
138	0	15	300	7(0.4)18	0(2)30	19
144	0	15	300	7(0.4)18	0(2)30	19
148	0	15	300	7(0.4)18	0(2)30	19
139	0	15	85	0.5(0.1)36	1(2)29	17
146	0	15	85	0.5(0.1)36	1(2)29	17
137.5	0	15	300	5(0.1)20	1(2)29	17
144.5	0	15	300	5(0.1)20	1(2)29	17
70	0	25	300	7(0.4)18	10(2)40	19
76	0	25	300	7(0.4)18	10(2)40	19
82	0	25	300	7(0.4)18	10(2)40	19
155	0	25	300	7(0.4)18	10(2)40	19
161	0	25	300	7(0.4)18	10(2)40	19
167	0	25	300	7(0.4)18	10(2)40	19
171	0	25	300	7(0.4)18	10(2)40	19
69	0	12	300	7(0.4)18	3(2)23	19
69	0	12	300	9.5(0.1)11.5	4(1)13	19
76	0	12	300	7(0.4)18	3(2)23	19
76	0	12	300	9.5(0.1)11.5	4(1)13	19
70.5	15	15	300	6(0.1)20	1(2)29	17
77.5	15	15	300	6(0.1)20	1(2)29	17
71.5	15	15	100	6(0.1)20	1(2)29	17
139.5	15	15	300	6(0.1)20	1(2)29	17
141.5	15	15	100	6(0.1)20	1(2)29	17
71	18.4	13	300	7(0.4)19	2(2)24	19
71	18.4	13	300	9.5(0.1)11.5	4(1)13	19
78	18.4	13	300	7(0.4)18	2(2)24	19
78	18.4	13	300	9.5(0.1)11.5	4(1)13	19
134	26.6	15	300	7(0.4)18	0(2)30	19
140	26.6	15	300	7(0.4)18	0(2)30	19
146	26.6	15	300	7(0.4)18	0(2)30	19
150	26.6	15	300	7(0.4)18	0(2)30	19

TABLE III. ILEED intensity data for the (00) beam of electrons diffracted from Al(100) used in the analysis of surface-plasmon dispersion reported in Secs. III and IV. Last two columns give the optical potential parameters used in the analysis of the data.

E (eV)	ϕ (deg)	θ (deg)	T (°K)	Δw (eV)	Data reference	ELEED parameters V_0 (eV)	λ_{ee} (Å)
69	0	12	300	0.1	19	16.5	8.5
76	0	12	300	0.1	19	16.5	8.5
138	0	15	300	0.4	19	16.5	11.0
144	0	15	300	0.4	19	16.5	11.0
76	0	25	300	0.4	19	21.0	10.0
82	0	25	300	0.4	19	21.0	10.0
161	0	25	300	0.4	19	14.7	11.7
167	0	25	300	0.4	19	14.7	11.7
70.5	15	15	300	0.1	17	16.7	7.5
77.5	15	15	300	0.1	17	16.7	7.5

shown in Fig. 1. The inelastic scattering vertices and associated plasmon propagators are given by Eqs. (4)–(10) in Ref. 22. Reference 22 also contains descriptions of the bulk-plasmon propagators [Eqs. (11)–(12) and the discussion thereof] used in our analysis; of the expressions for the ILEED cross sections [Eqs. (16)–(20)]; and of the expressions for the complex one-electron "optical" potential in which the incident electron moves inside the solid [Eqs. (14) and (15)].

The body of our analysis consists of calculating the ILEED intensities as functions of the parameters specified above and those which characterize the surface-plasmon dispersion relation, i.e.,

$$\hbar\omega_s(p_\parallel) = \hbar\omega_s + C_1 p_\parallel + C_2 p_\parallel^2, \tag{1a}$$

$$\Gamma_s(p_\parallel) = \Gamma_s + D_1 p_\parallel. \tag{1b}$$

The parameters $\hbar\omega_s$, C_1, C_2, Γ_s, and D_1 are varied until the calculated intensities are brought into correspondence with the observed ones in accordance with the criteria described in connection with Eq. (7) in Duke and Landman.[25]

The analysis is carried out in four steps. First, we select the data to be analyzed: a topic which we shall discuss further. Second, the incoherent (phonon- and defect-assisted) background is estimated for incorporation into the model calculations. Third, we evaluate the plasmon damping parameters Γ_s and D_1. Finally, given Γ_s, D_1, and all of the other parameters, those describing surface-plasmon dispersion, i.e., $\hbar\omega_s$, C_1, and C_2, are obtained by virtue of constructing plots of the "regions of ambiguity" as defined in Refs. 23–25. The results for Al(100) proved sufficiently similar to those of Al(111) that we did not carry out the detailed self-consistency check of the initial values of Γ_s and D_1 which was performed for Al(111).[25]

Turning to our selection of the incident beam parameters for which to perform the ILEED measurements, we recall that this choice is based on selecting sets of (E, θ, ϕ) values in the vicinity of energy-tuned elastic scattering ("Bragg") resonances in the elastic diffraction intensities. For the two-step model to provide a precise description of the ILEED intensities, the single-scattering ("kinematical") model should yield an accurate description of the elastic-low-energy-electron-diffraction (ELEED) intensities over a range of incident beam parameters near those characteristic of the resonant elastic maximum ($E = E_B$, $\theta = \theta_B$). This requirement is least stringent when the ILEED analysis is carried out at the two incident beam energies $E = E_B$, $E_B + \hbar\omega_s(p_\parallel = 0)$, because in these cases one of the two (diffraction-before-loss or loss-before-diffraction) terms in the ILEED cross sections dominates the calculated results. Indeed, if we examine the observed ILEED intensities for the incident beam parameters

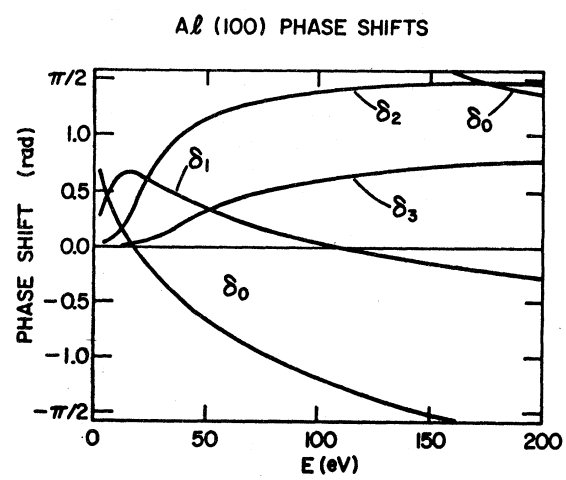

FIG. 1. Phase shifts for the ion cores in aluminum, calculated using an overlapping atomic charge density model (Ref. 29), utilized to specify the elastic scattering vertex [Eq. (4) in Ref. 23] for the two-step model of inelastic diffraction.

(E_B, θ_B, ϕ), then the elastic scattering vertex acts as a simple scale factor in the two-step model [see, e.g., Eq. (18) in Bagchi and Duke[22]], so that only the correct location of the resonant maximum at $E=E_B$, $\theta=\theta_B$ is of significance. Thus, we anticipate that almost any model of the elastic scattering resonances will suffice for an analysis of surface-plasmon dispersion at the diffraction-before-loss $(E=E_B, \theta=\theta_B)$ resonance condition. The two-step model, however, will yield an adequate description of a loss-before-diffraction $(E=E_B+\hbar\omega_s, \theta'=\theta_B)$ ILEED resonance only if the associated experimental ELEED maximum changes with θ and E in accordance with the kinematical formulas

$$k_\perp(\vec{g}, E_B)+k_\perp(0, E_B)=2\pi n/d, \tag{2a}$$

$$k_\perp^2(\vec{g}, E)=k^2(E)-(\vec{k}_\parallel+\vec{g})^2, \tag{2b}$$

$$k^2(E)=(2m/\hbar^2)\{E+V_0 + i(\hbar^2/m\lambda_{ee})[(2m/\hbar^2)(E+V_0)]^{1/2}\}, \tag{2c}$$

$$k_\parallel(E, \theta)=(2mE/\hbar^2)^{1/2}\sin\theta, \tag{2d}$$

in which n is an integer (the "order" of the resonance maximum), d is the layer spacing, $\vec{g}$ is the reciprocal-lattice vector associated with the exit beam, V_0 is the real part of the one-electron self-energy,[30] and λ_{ee} is the one-electron penetration depth.[30] Consequently, in order to analyze ILEED data at a loss-before-diffraction resonance we first must verify that the resonance peak in the observed ELEED intensities satisfies Eqs. (2) for a fixed set of values for V_0 and λ_{ee} over a range of energy and angle: $E_B-2\text{ eV}\lesssim E\lesssim E_B+2\text{ eV}$; $\theta_B-3°\lesssim\theta\lesssim\theta_B+3°$. If, moreover, a resonance maximum satisfies Eqs. (2) over a wide range of energy and angle ($\Delta E\sim 10$ eV, $\Delta\theta\sim 10°$), then the two-step model can be utilized to analyze ILEED intensities over a range of incident beam energies $E_B-\frac{1}{2}\hbar\omega_s\lesssim E\lesssim E_B+\hbar\omega_s$, $\theta=\theta_B$ provided that no other prominent ELEED resonances occur in this region of values of the incident beam parameters.

The ELEED intensity data from Al(100), reported in Table I, were examined to locate kinematical resonance maxima by virtue of plotting the energies of prominent maxima versus $\cos^{-2}\theta$. If Eq. (2a) is satisfied for the specular beam, then $E_B(n)$ satisfies

$$E_B(n)=[-V_0+(\hbar^2\pi^2/2md^2)n^2]/\cos^2\theta. \tag{3}$$

Thus, plots of E_B vs $\cos^{-2}\theta$ should yield straight lines for each value of the integer n. Typical plots for the $\phi=0$ azimuth are shown in Fig. 2. The solid lines in this figure indicate the predictions of Eq. (3) using $V_0=15$ eV and the bulk lattice spacing of Al(100): $d=2.0201$ Å. [This is an adequate model for Al(100) because the surface and bulk lattice spacings are equal[18,31–33] to within 0.1 Å.]

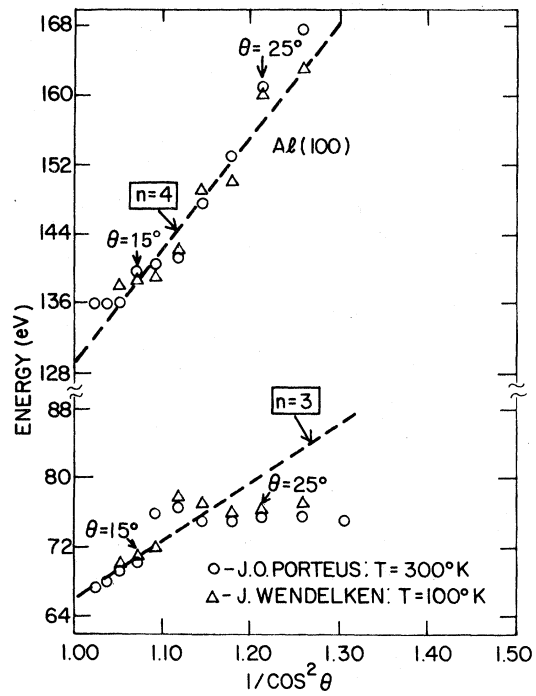

FIG. 2. Plots of the energies of prominent peaks in the $\theta=0$ ELEED intensities from Al(100) as a function of the reciprocal of the square of the cosine of the incident angle. Open circles are obtained from the room-temperature data of Porteus (Ref. 19). Closed circles are obtained from the $T=100$ °K data of Wendelken (Ref. 17). Straight lines indicate kinematical behavior associated with the bulk lattice spacing, $d=2.0201$ Å, and an inner potential of $V_0=15$ eV. It is known (Refs. 17 and 31–33) that the upper layer spacing of Al(100) is identical to that of the bulk within 0.1 Å.

It is evident from the figure that the only precisely kinematical behavior is exhibited by the $n=3$ Bragg resonance ($E_B\cong 70$ eV) in the angular range $9°\lesssim\theta\lesssim 17°$. The $n=4$ ($E_B\cong 138$ eV) resonance is approximately kinematical over the angular range $5°\lesssim\theta\lesssim 27°$. The $n=3$ peak behaves dynamically for values of $\theta\geq 19°$. These results are, moreover, roughly independent of the azimuthal angle,[17,19] so that Fig. 2 is representative of the behavior exhibited by the entire data base indicated in Table I.

Once we have selected the ELEED resonances suitable for obtaining and analyzing the associated ILEED data, the ILEED intensities are measured and kinematical-model descriptions of the ELEED intensities in the vicinity of this resonance are constructued. Typical examples of these descriptions for the resonances at $\phi=0$, $\theta=15°$, $25°$ are shown in Fig. 3. The model calculations were performed using the phase shifts shown in Fig. 1 and the optical-potential parameters given in Table III. The kinematical model usually describes the observed resonances for $E_B-5\text{ eV}\leq E\leq E_B+5$

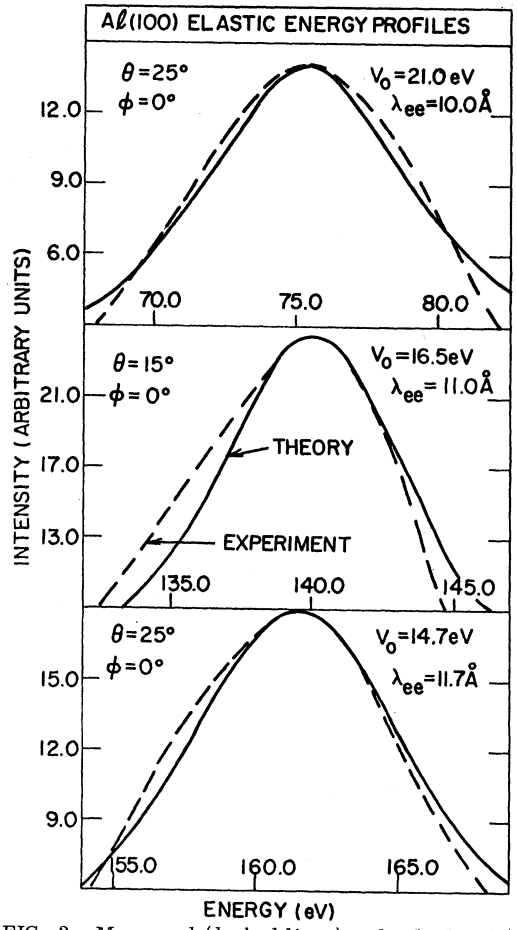

FIG. 3. Measured (dashed lines) and calculated (solid lines) elastic-low-energy-electron-diffraction intensities from Al(100) in the vicinity of prominent resonances. Theoretical curves were calculated using a single-scattering approximation (the Born approximation) which incorporates the phase shifts shown in Fig. 1 and the optical-potential parameters listed in Table III. The $\theta=0$ azimuth lies along a side of the primitive unit mesh on Al(100).

eV for a fixed value of $\theta=\theta_B$. Only for $E\sim 70$ eV, $\phi=0$, 15°, $9°\leq\theta\leq 17°$, however, is the behavior of the peak energy as a function θ predicted adequately by this model (see, e.g., Fig. 2).

Having determined the one-electron optical potential (V_0, λ_{ee}) from the observed ELEED intensity data, our final preliminaries prior to evaluating the surface-plasmon dispersion ($\hbar\omega_s, C_1, C_2$) are those of fixing the parameters describing the incoherent inelastic scattering background and the surface-plasmon damping (Γ_s, D_1). The former is accomplished in the manner described by Duke and Landman[25] leading to the expression for the background

$$\left(\frac{d\sigma}{d\Omega\, d\epsilon}\right)_{\text{incoh}} = 0.05 + 0.017/(\theta' + 0.01). \qquad (4)$$

The plasmon damping parameters were obtained primarily by analyzing the linewidths of the surface-plasmon peaks in the loss profiles as a function of θ' for the two resonances at $\phi=0$, $\theta=15°$. We obtain

$$\Gamma_s(p_\parallel) = 1.2(\pm 0.5) + 1(\pm 0.5)p_\parallel, \qquad (5)$$

in which energies are measured in eV and momenta in reciprocal angstroms. Equations (4) and (5) specify all of the remaining parameters in the model except those ($\hbar\omega_s, C_1, C_2$) characterizing surface-plasmon dispersion. Thus, it is the determination of these final three parameters to which we turn in the Sec. IV.

IV. SURFACE-PLASMON DISPERSION

We recall from earlier considerations[21–25] of surface-plasmon dispersion on Al(111) that the central problem in the determination of $\hbar\omega_s$, C_1, and C_2 in Eq. (1a) is the large number of values of these parameters consistent with the inelastic-low-energy-electron-diffraction (ILEED) intensities associated with a given elastic-low-energy-electron-diffraction (ELEED) resonance. Therefore it is desirable to analyze ILEED intensities associated with several ELEED resonances in order to obtain the reduced range of values of ($\hbar\omega_s$, C_1, C_2) which describes *all* of the data. The results of such analyses may be presented conveniently as plots of those values of C_1 and C_2, for fixed $\hbar\omega_s$, for which the maxima in the ILEED loss profiles are predicted to within the resolution of the experimental data (i.e., $\delta w \geq 0.1$ or 0.4 eV for the data summarized in Tables II and III). For each incident beam configuration (i.e., set of E, θ, ϕ) those values of C_1 and C_2 consistent with all of the associated ILEED intensities are displayed as "regions of ambiguity" in a two-dimensional C_1–C_2 plane,[23–25] one such region being displayed for each triplet of (E, θ, ϕ) values. The union of these regions for all (E, θ, ϕ) specifies that range of values of C_1 and C_2, obtained with a fixed value of $\hbar\omega_s$, which is compatible with all of the ILEED intensity data. By performing such analyses for various $\hbar\omega_s$ we can map out the volume of the three-dimensional $\hbar\omega_s$-C_1-C_2 space consistent with the ILEED observations.

The first step in this process is the estimation of $\hbar\omega_s$ via inspection of the peak energies w_p of the loss profiles for $\theta'\sim\theta$ (i.e., $p_\parallel\cong 0$). This initial examination already suggests pronounced differences between surface-plasmon dispersion on Al(100) and that on Al(111). In the latter case, $\omega_p(\theta'\cong\theta)\geq 10.4$ eV for all measured loss profiles, with w_p $(\theta'\cong\theta)\geq 10.5$ eV for diffraction-before-loss resonance energies ($E=E_B$). This observation establishes $\hbar\omega_s\cong 10.5$ eV for Al(111), as reported in Refs. 24 and 25. In the present case of Al(100),

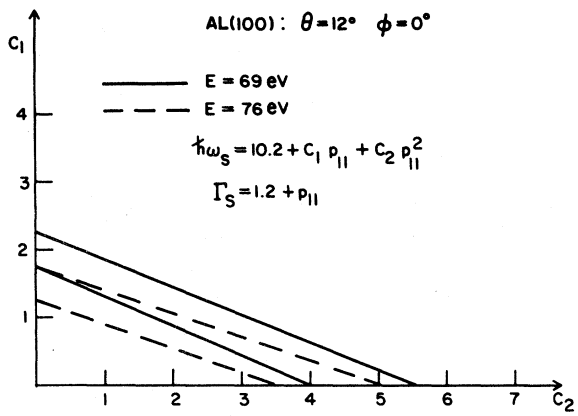

FIG. 4. Regions of ambiguity in the surface-plasmon dispersion relation of Al(100) associated with the ELEED resonance at ($E_B = 69$ eV, $\theta = 12°$, $\phi = 0$). Calculations were performed using $\hbar\omega_s = 10.2$ eV, $\Gamma_s = 1.2 + p_\parallel$, the phase shifts shown in Fig. 1, and the optical potential parameters given in Table III. Data analyzed are specified in Table III. Any dispersion relation with values of C_1 and C_2 lying between the two lines associated with $E = 69$ eV (solid lines) and $E = 76$ eV (dashed lines) yields an adequate two-step model description of the observed ILEED loss profiles.

however, for diffraction-before-loss (DL) resonances we find the minimum value of w_p in the range

$$10.15 \leq w_p^{\mathrm{DL}} \leq 10.25 \text{ eV}, \tag{6}$$

whereas for the loss-before-diffraction (LD) resonances

$$9.8 \leq w_p^{\mathrm{LD}} \leq 10.25 \text{ eV}. \tag{7}$$

The large range of w_p^{LD} values reflects the importance of elastic diffraction phenomena in determining the peak in the loss-before-diffraction loss profiles.[22] Nevertheless, it is clear from Eqs. (6) and (7) without any analysis at all that if $C_1 > 0$ and $C_2 > 0$, then we must select $\hbar\omega_s$ in accordance with $9.9 \leq \hbar\omega_s \leq 10.3$ eV: a range which does not include the 10.5 eV value obtained for Al(111).

Another surprise also confronted us, however, upon inspection of the ILEED intensity data. Rather than increase monotonically with increasing $p_\parallel$, the peak energies $w_p(\theta')$ of the loss profiles associated with the DL ($E = E_B$) resonances initially *decreased* as $p_\parallel$ is increased from zero for $p_\parallel \lesssim p_\parallel^{(0)}$, $0.1 \lesssim p_\parallel^{(0)} \lesssim 0.2$ Å^{-1}, prior to their subsequent increase with increasing $p_\parallel$. This behavior cannot be attributed to elastic diffraction phenomenon, and suggests a negative value of C_1, i.e.,

$$C_1 \cong -2C_2 p_\parallel^{(0)}. \tag{8}$$

This fact, together with the expectation that $\hbar\omega_s$ should be independent of crystal face suggests the use of $\hbar\omega_s \sim 10.4$ eV and $C_1 < 0$ for Al(100).

Independent of the above considerations which indicate that $C_1 < 0$, we undertook to construct the regions of ambiguity in the $C_1 - C_2$ plane for the best "compromise" value of $\hbar\omega_s = 10.2$ eV in analogy with our procedure for Al(111).[25] These are shown in Figs. 4–8 for the ILEED intensity data summarized in Table III. Indeed, the shape of these regions differs markedly from those obtained for[24,25] Al(111) in that the regions of ambiguity for the LD resonances as well as the DL resonances extend to large values of $4 \lesssim C_2 \lesssim 5$ eV Å^2 as $C_1 \to 0$. The only exception to this result occurs for the LD resonance at (167 eV, 25°, 0). The ILEED data analysis for this LD resonance is not a reliable consequence of the two-step model, however, because the ELEED resonance at (162 eV,

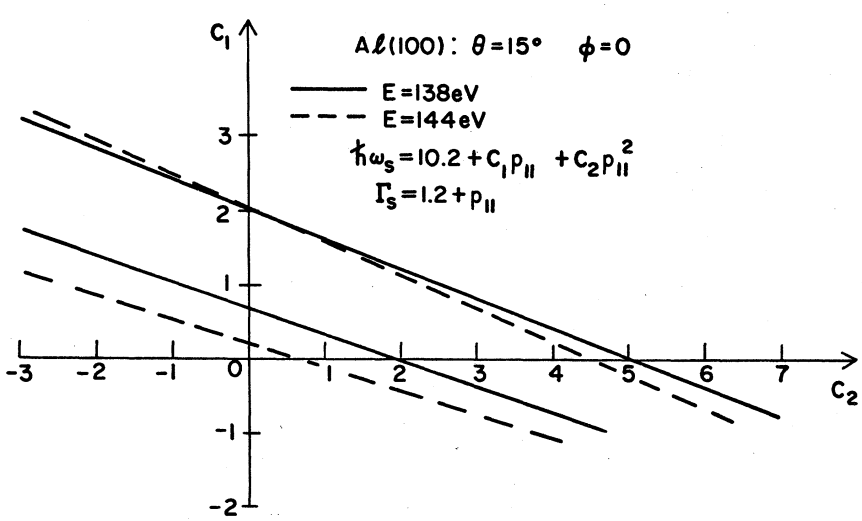

FIG. 5. Regions of ambiguity in the surface-plasmon dispersion relation of Al(100) associated with the ELEED resonance at ($E_B = 139$ eV, $\theta = 15°$, $\phi = 0$). Calculations were performed using $\hbar\omega_s = 10.2$ eV, $\Gamma_s = 1.2 + p_\parallel$, the phase shifts shown in Fig. 1, and the optical potential parameters given in Table III. Data analyzed are specified in Table III. Any dispersion relation with values of C_1 and C_2 lying between the two lines associated with $E = 138$ eV (solid lines) and $E = 144$ eV (dashed lines) yields an adequate two-step model description of the observed ILEED loss profiles.

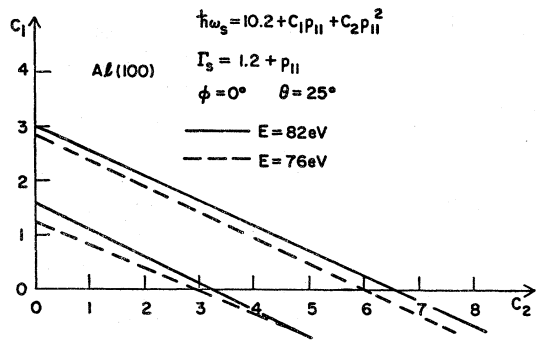

FIG. 6. Regions of ambiguity in the surface-plasmon dispersion relation of Al(100) associated with the ELEED resonance at ($E_B = 76$ eV, $\theta = 25°$, $\phi = 0$). The calculations were performed using $\hbar\omega_s = 10.2$ eV, $\Gamma_s = 1.2 + p_{\parallel}$, the phase shifts shown in Fig. 1, and the optical potential parameters given in Table III. Data analyzed are specified in Table III. Any dispersion relations with values of C_1 and C_2 lying between the two lines associated with $E = 82$ eV (solid lines) and $E = 76$ eV (dashed lines) yields an adequate two-step model description of the observed ILEED loss profiles.

25°, 0) does not behave kinematically as is evident from Fig. 2. In fact, the reliable two-step analyses of LD resonances are those at (76 eV, 12°, 0) and (77.5 eV, 15°, 15°) shown in Figs. 4 and 8, respectively. Both are consistent with $C_1 = 0$ and $4 \leq C_2 \leq 5$ eV Å^2.

The important feature of Figs. 4–8 is their conversion of the loss-profile maxima as functions of θ', i.e., $w_p(\theta')$, into a range of plasmon dispersion relations

$$\hbar\omega_s(p_{\parallel}) = 10.2(\pm 0.1) + 1.5(\pm 0.5)p_{\parallel} + 0(+2)p_{\parallel}^2, \qquad (9a)$$

consistent with the loss-profile data. Energies are measured in eV and momenta in reciprocal angstroms. The reliable loss-profile data span the range of values $p_{\parallel} \lesssim 0.5$ Å^{-1} being accessed experimentally for $\theta' < \theta$. Essentially only one loss profile, that for $\theta' = \theta + 1°$, yields peak energies for plasmon momenta close to $p_{\parallel} = 0$. In the fitting procedure leading to Eq. (9a) the maximum resulting from this loss profile is not unusually heavily weighted. If we require that $\hbar\omega_s$ for Al(100) be compatible with that for Al(111), however, and further use negative values of C_1 via Eq. (7) as a vehicle to accomplish this objective, then we obtain the dispersion relation

$$\hbar\omega_s(p_{\parallel}) = 10.4(\pm 0.1) - 2(\pm 1)p_{\parallel} + 9(\pm 3)p_{\parallel}^2. \qquad (9b)$$

This result is, for practical purposes, equivalent to Eq. (9a) *except for the* $\theta' = \theta + 1°$ *loss profile for* which it predicts a rather larger value of $w_p(\theta')$. Otherwise, over the range $p_{\parallel} \leq 0.4$ Å^{-1} Eqs. (9a) and (9b) map out comparable regions of the $\hbar\omega_s$-vs-$p_{\parallel}$ plane. The larger predicted values of $w_p(\theta + 1°)$ resulting from Eq. (9b) are generally in better agreement with the DL resonance loss profiles and in poorer agreement with the $E = E_B + 5$–6 eV loss profiles. Finally, the extremes in Eq. (9b) reached by use of independent error increments [e.g., $\hbar\omega_s(p_{\parallel}) = 10.5 - p_{\parallel} + 12p_{\parallel}^2$] lie well outside the region spanned by Eq. (9a). Therefore the error estimates in Eq. (9b) should be performed in a complimentary sense (e.g., decreasing C_1 is accomplished by increasing C_2, etc.) as discussed by Bagchi and Duke.[22]

V. SYNOPSIS AND DISCUSSION

Two types of results emerge from the analysis presented above. First, several refinements have been added to our previously developed[23–26] methodology for extracting surface-plasmon dispersion relations from observed inelastic-low-energy-electron-diffraction (ILEED) intensities. Second, we have performed the first determination of this dispersion relation for Al(100), and presented the results in Eq. (5) and (9). In this section, we discuss the origin and consequences of the revision in our methodology, and the interpretation of our results.

The refinements in our analytical procedure stem from an increased awareness of the limitations of the two-step model.[27,34] Specifically, unless either the diffraction-before-loss (DL) processes dominate (i.e., $E = E_B$) or the observed elastic-low-energy-electron-diffraction (ELEED) intensities behave kinematically [i.e., satisfy Eqs. (2)] in the vicinity of a resonance, the two-step model overestimates the influence of elastic diffraction phenomena on the ILEED loss profiles. For example, for Al(100) we find that the two-step

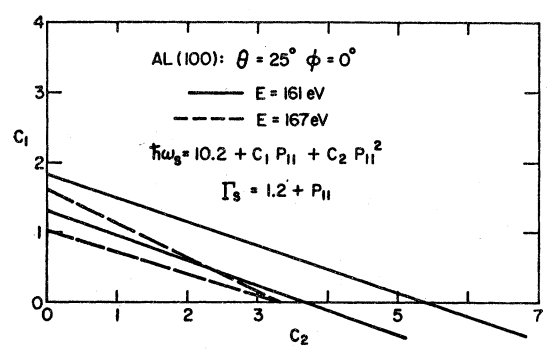

FIG. 7. Regions of ambiguity in the surface-plasmon dispersion relation of Al(100) associated with the ELEED resonance at ($E_B = 161$ eV, $\theta = 25°$, $\phi = 0$). Calculations were performed using $\hbar\omega_s = 10.2$ eV, $\Gamma_s = 1.2 + p_{\parallel}$, the phase shifts shown in Fig. 1, and the optical potential parameters given in Table III. Data analyzed are specified in Table III. Any dispersion relation with values of C_1 and C_2 lying between the two lines associated with $E = 161$ eV (solid lines) and $E = 167$ eV (dashed lines) yields an adequate two-step model description of the observed ILEED loss profiles.

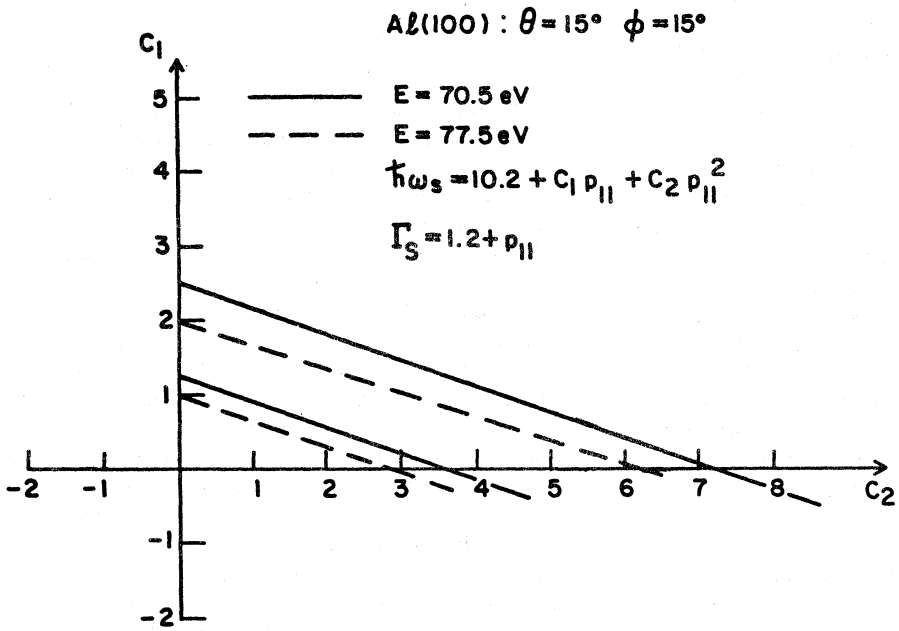

FIG. 8. Regions of ambiguity in the surface-plasmon dispersion relation of Al(100) associated with the ELEED resonance at (E_B =70.5 eV, θ =15°, ϕ =15°). Calculations were performed using $\hbar\omega_s$ =10.2 eV, Γ_s =1.2 + $p_{\parallel}$, the phase shifts shown in Fig. 1, and the optical potential parameters given in Table III. Data analyzed are specified in Table III. Any dispersion relation with values of C_1 and C_2 lying between the two lines associated with E =70.5 eV (solid lines) and E =77.5 eV (dashed lines) yields an adequate two-step model description of the observed ILEED loss profiles.

model misplaces the peak in the loss profile, relative to a complete multiple scattering calculation,[35] by as much as 0.5 eV in adverse circumstances. An earlier study[36] of the effect led to smaller peak shifts ($\Delta\omega_p \leq 0.1$ eV) of the two-step relative to the dynamical model because of the use of a weaker scattering potential in the calculations.

In order to circumvent errors created by this situation, we adopted two changes in our analysis. First, we examined the behavior of prominent ELEED resonance maxima as functions of incident angle θ as well as energy, discerning kinematical behavior by plotting the peak energy versus $(\cos^2\theta)^{-1}$ as shown in Fig. 2. Indeed, one of the striking consequences of the examination of the two good examples of kinematical ELEED behavior, (see Figs. 4 and 8) is the occurrence for $\hbar\omega_s = 10.2$ eV of the maximum overlap between the DL and LD regions of ambiguity at large values of $4 \lesssim C_2 \lesssim 6$ eV Å^2 and $0 \leq C_1 < -1$ eV Å: a marked contrast to the occurrence of this region near $1 \lesssim C_2 \lesssim 2$ eV Å and $C_2 \sim 0$ in the other cases (see Figs. 5–7) for Al(100) and for Al(111).[23–25] Second, given the result[35] that comparison of the dynamical and two-step models revealed that for $\theta' \lesssim \theta$ and $E = E_B$ the maxima in the loss profiles differ by $\Delta w_p \lesssim 100$ meV even for Al(100), we focused our attention on the DL($E = E_B$) resonances at the other angles of incidence (Figs. 5–7). Following this procedure, we obtained a composite region of ambiguity consistent with that predicted by the two kinematical resonances. It is noteworthy that preliminary calculations[35] indicate that for $E = E_B$ the kinematical model underestimates $w_p(\theta')$ whereas for $E = E_B$ +5–6 eV it overestimates $w_p(\theta')$. Therefore in Figs. 4–8 the solid regions move toward smaller $C_1 - C_2$ values whereas the dashed lines shift to larger values of $C_1 - C_2$; i.e., the two regions of ambiguity shown in each figure tend to merge.

These new insights into the methodology have direct consequences for our previous analysis of surface-plasmon dispersion Al(111). Most notably, they lead us to disregard the LD resonance analyses in Figs. 8, 9, and 11 of Ref. 25 because we did *not* verify their kinematical character. The resulting plasmon dispersion relation is of the form [for Al(111)]

$$\hbar\omega_s(p_{\parallel}) = 10.5 + C_1(\pm 0.5)p_{\parallel} + C_2(\pm 0.5)p_{\parallel}^2, \quad (10a)$$

$$2.6\,C_1 + C_2 = 6.5; \quad C_2 > 0, \quad C_1 \gtrsim -1, \quad (10b)$$

$$\Gamma_s(p_{\parallel}) = 1.85(\pm 1) + 3(\pm 2)p_{\parallel}. \quad (10c)$$

Equations (10) illustrate an important result: Until further studies of the ELEED intensities from Al(111) are performed to verify the kinematical behavior of resonances suitable for LD analyses, the region of the C_1–C_2 plane in the vicinity of $C_1 = -1$ eV Å, $C_2 = 9$ eV Å^2 can no longer be eliminated as was thought to be the case in Refs. 24 and 25.

We now come to the major topic of this section, the interpretation of the surface-plasmon dispersion relations given by Eqs. (5), (9), and (10). Turning first to the consistency of our results for Al(100) with those for Al(111) and with the literature, we note that if Eq. (9b) is used to describe surface-plasmon dispersion on Al(100), then $\hbar\omega_s(p_{\parallel} = 0)$ is the same for Al(100) as for Al(111) within experimental uncertainties. Moreover, our

result for $\hbar\omega_s(p_{\parallel}=0)$ is in satisfactory correspondence with that obtained of Kloos and Raether[37] on the basis of keV electron transmission through thin, polycrystalline foils. Indeed, on the basis of random-phase-approximation (RPA) analyses of uniform electron-fluid models we would expect[38] $\hbar\omega_s(p_{\parallel}=0)$ to the independent of the electron-density profile at the surface and, consequently, to be identical for polycrystalline film and all single-crystal faces of a given material. Preliminary analyses[39] indicate that this result is a general consequence, independent of the model of the positive charges associated with the ion cores.

The interpretation of our results for Γ_s, C_1, and D_1 is more complicated. Four influences on these quantities have been identified in the literature: (i) bulk interband transitions,[40] (ii) electron collisions with impurities and lattice vibrations,[41–45] (iii) loss of electron phase coherence upon reflection from the "surface,"[45,46] and (iv) the shape of the electron density profile at the surface[4–11,47–51] (assuming no electronic loss of phase coherence upon reflection at the surface). Unfortunately, however, a definitive assessment of the relative importance of these four phenomenon has not yet emerged because of two major difficulties. First, all four effects have not been examined simultaneously within the context of a given model. Second, the various model calculations embody different technical approximations, the consequences of which cannot be separated from those of the models themselves. Thus, we focus our discussion on the general implications of our results concerning the types of phenomenon which should be included in realistic microscopic models of surface plasmon dispersion.

The outstanding attribute of our results for $\Gamma_s = 1.2 \pm (0.5)$ eV is its enhancement relative to the corresponding value,[20–22] $\Gamma_b = 0.53$ eV, for bulk plasmons. Although naively one might ascribe this phenomenon to the electrons' loss of phase coherence from boundary scattering, Zaremba's kinetic-theory analysis[45] indicates that within the context of his model such scattering enhances D_1 but leaves Γ_s *unaffected* (subject to the boundary condition of zero current flow normal to the surface). The apparent temperature dependence of the surface-plasmon dispersion relation observed by Wendelken[17] suggests that phonon-induced broadening of the scattered beam is a possible candidate for the origin of this additional width. Since the rms vibrations of surface atoms are at least twice those associated with corresponding bulk species,[28] electron-phonon scattering at the surface is substantially larger than in the bulk.

Turning to our expressions [Eqs. (5), (9), and (10)] for C_1 and D_1, we find two regions of admissible values:

$$C_1 \sim D_1 \sim 2 \text{ eV Å}; \quad C_2 \cong 0, \tag{11a}$$

$$-C_1 \sim D_1 \sim 2 \text{ eV Å}; \quad C_2 \cong 9 \text{ eV Å}^2. \tag{11b}$$

Equation (11a) is preferred for Al(111) and Eq. (11b) for Al(100). The important feature of Eqs. (11) is that of $C_1 > 0$ then $C_2 \cong 0$, whereas if $C_1 < 0$ then C_2 is large. This result reflects a fundamental ambiguity inherent in the interpretation of ILEED intensity data, as may be seen clearly from Figs. 4–8.

The facts that Γ_s is finite and D_1 is large, i.e., $D_1 \gtrsim |C_1|$, immediately eliminate all existing models without bulk electron-defect collisions as serious candidates for data interpretation. Specifically, Zaremba[45] demonstrates that using the Vlasov equation to describe boundary scattering alone (from a step electron density) yields $\Gamma_s = 0$, $D_1 \lesssim \frac{1}{2}C_1$ and $C_1 \cong 6 \pm 0.5$ eV Å: all three results being manifestly inconsistent with both of Eqs. (11). Similarly, the infinite-wall random-phase-approximation (RPA) analyses[50,52–55] predict $\Gamma_s = 0$, $D_1 \lesssim \frac{1}{20}C_1$ and $C_1 = 4.3$ eV Å, also inconsistent with the results of our analysis. The high-frequency step-density RPA analysis leads[52,56] to $\Gamma_s = C_1 = 0$. The only systematic consideration of bulk electron scattering processes has been given only by Heinrichs[42,43] within the context of an approximate "dielectric-approximation" step-density hydrodynamic model analysis. He finds $C_1 = 3.18$ eV Å and $D_1 = 6.34$ eV Å. Both of these values are too large to be consistent with Eqs. (5) and (10). Therefore in spite of the approximate nature of both this and the other models, we conclude that descriptions both of electronic scattering processes from defects and phonons, and of the spatial distribution of the surface electronic charge density are necessary ingredients in realistic models of surface-plasmon dispersion. Moreover, it is evident from Eqs. (5), (9), and (10) (or Figs. 4–8) that only an uncertainty in the relative magnitudes of C_1 and C_2 remains unresolved for both Al(111) and Al(100). Thus, calculations of C_1 and D_1 alone are inadequate to resolve the sort of ambiguities which seem inherent in analyses of ILEED intensity data. Values of Γ_s, C_2, and D_2 also must be evaluated.

In summary, therefore, we have identified an additional limitation on the application of two-step model to analyze ILEED intensity data; i.e., that the kinematical behavior of the associated ELEED resonance as a function of incident beam angle must be verified explicitly. This requirement was imposed for the present analysis of surface-plasmon dispersion on Al(100) leading to Eqs. (5) and (9) for the resulting dispersion relation. Imposing it *a posteriori* on our prior analysis for Al(111) led to the replacement of our earlier results[24,25] with the less restrictive Eqs. (10). Although the re-

sulting dispersion relations for Al(100) and Al(111) are not as conclusive as we would like, they demonstrate that models which embody an adequate description of the surface scattering processes and electronic charge are *essential* to achieve an interpretation of the ILEED data. Finally, our results indicate clearly that model calculations of the linear term in the dispersion relation alone are destined for an inconclusive verification. The ILEED data determine most accurately the relationship between C_1 and C_2 [see, e.g., Eq. (8)], not the values of C_1 or C_2 independently. In this sense, we were able to establish that the surface-plasmon dispersion on Al(100) is "flatter" than on Al(111) (e.g., smaller C_1 for $C_2 \equiv 0$) and is less heavily damped (i.e., $\Gamma_s[\mathrm{Al}(100)] < \Gamma_s[\mathrm{Al}(111)]$, $D_1[\mathrm{Al}(100)] < D_1[\mathrm{Al}(111)]$). On balance, therefore, while the precision of the results is disappointing to us, it is sufficient to demonstrate the inadequacy of existing "microscopic" descriptions of surface-plasmon dispersion, to reveal the directions in which such model calculations should be refined, and to display a systematic difference between surface-plasmon dispersion on Al(100) and Al(111).

ACKNOWLEDGMENTS

The authors are indebted to Dr. P. J. Feibelman for stimulating discussions, to Dr. U. Landman for assistance in performing preliminary dynamical ILEED intensity calculations using multiple-phase-shift elastic scattering vertices, and to Professor R. T. Chien and Professor F. M. Propst of the University of Illinois for advice and support. The able assistance of Jeanne Graham is gratefully acknowledged, as is the hospitality of Dr. F. Galeener and Dr. G. E. Pake of the Xerox Palo Alto Research Center where this manuscript was completed.

*Present address: Brown Boveri Research Center, Baden, Switzerland.

†Present address: Oak Ridge National Laboratory, Oak Ridge, Tenn. 37830.

[1]R. Smoluchowski, Phys. Rev. 60, 661 (1941).

[2]C. B. Duke, J. Vac. Sci. Technol. 6, 152 (1969).

[3]N. D. Lang, Solid State Phys. 28, 225 (1973).

[4]A. J. Bennett, Phys. Rev. B 1, 203 (1970).

[5]L. Kleinman, Phys. Rev. B 7, 2288 (1973).

[6]D. E. Beck and V. Celli, Phys. Rev. Lett. 28, 1124 (1972).

[7]P. J. Feibelman, Phys. Rev. Lett. 30, 975 (1973).

[8]P. J. Feibelman, Surf. Sci. 40, 102 (1973).

[9]H. L. Lemberg, S. A. Rice, P. H. Naylor, and A. N. Block, Solid State Commun. 14, 1097 (1974).

[10]S. A. Rice, D. Guidotti, H. L. Lemberg, W. C. Murphy, and A. N. Bloch, Adv. Chem. Phys. 27, 543 (1974).

[11]E. M. Conwell, Phys. Rev. B 11, 1508 (1975).

[12]J. O. Porteus and W. N. Faith, Phys. Rev. B 2, 1532 (1970).

[13]J. M. Burkstrand and F. M. Propst, J. Vac. Sci. Technol. 9, 731 (1972).

[14]J. O. Porteus and W. N. Faith, J. Vac. Sci. Technol. 9, 1062 (1972).

[15]J. M. Burkstrand, Phys. Rev. B 7, 3443 (1973).

[16]J. O. Porteus and W. N. Faith, Phys. Rev. B 8, 491 (1973).

[17]J. Wendelken, Ph. D. thesis (University of Illinois, 1974) (unpublished); Coordinated Science Laboratory Report (unpublished); Phys. Rev. B (to be published).

[18]J. O. Porteus, Surf. Sci. 41, 515 (1974).

[19]J. O. Porteus and W. N. Faith Phys. Rev. B (to be published).

[20]A. Bagchi, C. B. Duke, P. J. Feibelman, and J. O. Porteus, Phys. Rev. Lett. 27, 998 (1971).

[21]C. B. Duke and A. Bagchi, J. Vac. Sci. Technol. 9, 738 (1972).

[22]A. Bagchi and C. B. Duke, Phys. Rev. B 5, 2784 (1972).

[23]C. B. Duke and U. Landman, Phys. Rev. B 7, 1368 (1973).

[24]C. B. Duke, U. Landman, and J. O. Porteus, J. Vac. Sci. Technol. 10, 183 (1973).

[25]C. B. Duke and U. Landman, Phys. Rev. B 8, 505 (1973).

[26]C. B. Duke, U. Landman, L. Pietronero, and J. O. Porteus, Program of the Thirty-Fourth Conference on Physical Electronics, Bell Laboratories, New Jersey, 1974 (unpublished).

[27]G. E. Laramore and C. B. Duke, Phys. Rev. B 3, 3198 (1971).

[28]C. B. Duke, Adv. Chem. Phys. 27, 1 (1974).

[29]C. B. Duke, N. O. Lipari, and U. Landman, Phys. Rev. B 8, 2454 (1973).

[30]C. B. Duke and C. W. Tucker, Jr., Surf. Sci. 15, 231 (1969).

[31]C. B. Duke, G. E. Laramore, B. W. Holland, and A. M. Gibbons, Surf. Sci. 27, 523 (1971).

[32]G. E. Laramore and C. B. Duke, Phys. Rev. B 5, 267 (1972).

[33]M. R. Martin and G. A. Somorjai, Phys. Rev. B 7, 3607 (1973).

[34]C. B. Duke and G. E. Laramore, Phys. Rev. B 3, 3183 (1971).

[35]U. Landman and C. B. Duke (unpublished).

[36]C. B. Duke and U. Landman, Phys. Rev. B 6, 2968 (1972).

[37]T. Kloos and H. Raether, Phys. Lett. A 44, 157 (1973).

[38]P. J. Feibelman, Phys. Rev. B 3, 220 (1971).

[39]P. J. Feibelman (unpublished).

[40]J. M. Elson and R. H. Ritchie, Surf. Sci. 30, 178 (1972).

[41]D. Wagner, Z. Naturforsch. A 21, 634 (1966).

[42]J. Heinrichs, Phys. Rev. B 7, 3487 (1973).

[43]J. Heinrichs, Solid State Commun. 12, 167 (1973).

[44]V. V. Rumyantsev, Fiz. Tverd. Tela. 13, 2038 (1971) [Sov. Phys.-Solid State 13, 1709 (1972)].

[45]E. Zaremba, Phys. Rev. B 9, 1277 (1974).

[46]B. N. Libenson and V. V. Rumyantsev, Phys. Status Solidi B 65, 281 (1974).

[47]J. E. Inglesfeld and E. Wikborg, J. Phys. C 6, L 158 (1973).

[48]J. Harris and A. Griffin, Phys. Lett. A 34, 51 (1971).

[49]J. Harris and A. Griffin, Phys. Lett. A 37, 387 (1971).
[50]D. E. Beck, Phys. Rev. B 4, 1555 (1971).
[51]R. H. Ritchie and A. L. Marusak, Surf. Sci. 4, 234 (1966).
[52]P. J. Feibelman, C. B. Duke, and A. Bagchi, Phys. Rev. B 5, 2436 (1972).
[53]Ch. Heger and D. Wagner, Phys. Lett. A 34, 448 (1971).
[54]Ch. Heger and D. Wagner, Z. Phys. 244, 449 (1971).
[55]J. Harris, J. Phys. C 5, 1757 (1972).
[56]P. J. Feibelman, Phys. Rev. 176, 551 (1968).